IEEE Access
Multidisciplinary | Rapid Review | Open Access Journal

Received July 2, 2019, accepted July 30, 2019, date of publication August 6, 2019, date of current version September 16, 2019.

Digital Object Identifier 10.1109/ACCESS.2019.2933608

Design of Highly Uniform Magnetic Field Coils Based on a Particle Swarm Optimization Algorithm

WENFENG WU[1], BINQUAN ZHOU[1], ZHANCHAO LIU[1], JING WANG[1], HAOYING PANG[1], LINLIN CHEN[5], WEI QUAN[1,2,3,4], AND GANG LIU[1,2,3]

[1]School of Instrumentation and Optoelectronic Engineering, Beihang University, Beijing 100191, China
[2]Innovative Research Institute of Frontier Science and Technology, Beihang University, Beijing 100191, China
[3]Advanced Innovation Center for Biomedical Engineering, Beihang University, Beijing 100191, China
[4]Beijing Academy of Quantum Information Sciences, Beijing 100191, China
[5]Department of Aerospace Science and Technology, Space Engineering University, Beijing 101416, China

Corresponding authors: Binquan Zhou (bqzhou@buaa.edu.cn) and Zhanchao Liu (liuzhanchao@hotmail.com)

This work was supported in part by the Beijing Natural Science Foundation under Grant 4191002, in part by the BAQIS Research Program under Grant Y18G34, in part by the National Key Research and Development Program of China under Grant 2016YFB0501600, and in part by the National Natural Science Foundation of China under Grant 61773043, Grant 61673041, and Grant 61721091.

ABSTRACT An innovative design method is proposed for highly uniform magnetic field coils using a particle swarm optimization (PSO) algorithm. We use an optimization approach instead of the conventional method of solving closed-form equations to obtain the coil geometric parameters. We apply a PSO algorithm to the optimization of the coil structure and set an appropriate penalty function and boundary conditions. A discrete optimization is employed to avoid obtaining parameters with a large number of decimal places. Compared with the conventional design method, our method solves the problem of how to design a coil set to produce a highly uniform magnetic field under various structural and process constraints. The coil designed by this method can produce a highly uniform magnetic field for a larger effective space. This is significant for miniaturized applications, especially for miniature atomic sensors. The calculations show that the magnetic field deviations of the triaxial cylindrical coils designed by this innovative method are decreased by more than two orders of magnitude in the volume of interest (VOI) compared to conventional triaxial cylindrical coils. Our experimental measurements are consistent with theoretical values. Measurements show that relative magnetic field uniformities of the axial and radial coils reache 1.2×10^{-4} and 3.9×10^{-3} along the magnetic field axis in the range of $\pm 0.5R$. In addition, this method can also be used to design gradient field coils or other shaped coils.

INDEX TERMS Uniform magnetic field, triaxial cylindrical coil, PSO, miniature atomic sensors.

I. INTRODUCTION

Uniform magnetic fields are widely used in many fields of scientific research and in industry, such as for the measurement of the neutron electric dipole moments (nEDM), magnetic navigation systems (MNS), in vivo medical diagnostic studies, magnetic resonance imaging (MRI) [1]–[3]. All these precision measurements and precision controls require magnetic field with high uniformity. In nuclear magnetic resonance (NMR) applications, high-resolution experiments usually demand field homogeneities of a few parts per million within a volume of 0.5 cm^3 [4]. Miniature atomic sensors are a new type of sensor based on atomic physics and quantum mechanics. They have great development prospects due to high precision and small size. High precision measurements using miniature atomic sensors also require highly uniform magnetic fields. Therefore, it is our eternal pursuit to design coils with smaller volumes and larger region with uniform fields for miniature atomic sensors. Atomic sensors usually do not require too high magnetic field. A radial magnetic field of several hundred nT and an axial one of several tens of uT can meet the demand

The associate editor coordinating the review of this manuscript and approving it for publication was Sotirios Goudos.

of the NMR gyroscopes we studied. Therefore, the targeted magnetic field intensity can be achieved with a few coil turns. In this case, a single-turn structure is adopted. This means that the effect of wire dimensions (thickness, width, etc.) on the accuracy of the target field can be ignored. What we need to pay attention is how to reduce the overall size of the coil, such as the coil radius and coil height, while ensuring the uniformity of the magnetic field. As for the current density, it does not need to be too large. Under the size constraints in this paper, current of several mA is enough for the axial field and that of several uA is enough for the radial field. Non-uniform magnetic field (especially the axial non-uniform magnetic field) tends to cause the relaxation time to become shorter, which indirectly affects the accuracy of the sensor. In general, NMR gyroscopes with a cubic vapor cell of 4 mm side length require a radial magnetic field uniformity of better than several hundred ppm and axial magnetic field uniformity of several tens of ppm. On the one hand, under the same volume constraint, a more uniform magnetic field means that the sensor has the potential to achieve higher precision. On the other hand, under the same uniformity requirements, a more uniform magnetic field coil scheme has the possibility of reducing the coil volume, which is of great significance for miniature atom sensors. This is the original intention of our research on high uniform magnetic field coil design methods. Cylindrical coil structure is simple and convenient fabricate for creating triaxial magnetic fields. It is widely used in industrial equipment and medical instruments, and is also the first choice for miniature atomic sensors [5]–[7]. In a triaxial cylindrical uniform field coil configuration, Helmholtz coils and saddle coils are typically used to generate axial and radial magnetic fields, respectively. However, for both coils, generating a sufficiently uniform magnetic field within a specific size VOI comes at the expense of a large coil volume. In addition, it is well known that solenoids are usually used as radiofrequency coils in NMR. The longer the solenoid, the more uniform the magnetic field can be obtained. However, a miniature atomic sensor often requires a small coil length to diameter ratios. This obviously does not meet the needs of miniaturized applications such as miniature atomic sensors. It is particularly important to find a design method that has the flexibility to design coils according to application requirements (such as size, uniformity, etc.). Therefore, we propose an innovative design method using a PSO algorithm to address this problem.

Helmholtz coils are the most commonly used coils for axially uniform fields in industrial applications because of their simple construction. However, Helmholtz coils often fail to provide sufficiently uniform magnetic fields for high precision applications, including miniature atomic sensors. A Maxwell coil provides a more uniform magnetic field than a Helmholtz coil, but at the expense of requiring a more complex structure [8]. Systems of three or four identical air-core, circular coils for producing an extended uniform magnetic field were described by J. R. Barker in 1949 [9]. A four-coil system (including circular and square) consistent with the Barker four-coil structure was proposed by Lee-Whiting in 1957 [10]. Both coils have a non-integer number of ampere turns, which necessitates the use of two matched current sources. Synchronization between the two current sources increases the difficulty of the application. The ampere-turns of the Barker four-coil concept was approximately reproduced by J. L. Krischvink in 1992 [11]. However, this approximation results in a significant loss of magnetic field uniformity. Although P. Kedzia corrected the position of the Lee-Whiting circular coil to improve its magnetic field uniformity in [12], it is still inconvenient for miniaturized coils with an ampere-turn ratio of 9:4. In addition, M.W. Garrett proposed a series of coils to produce a uniform magnetic field, forming a mature theoretical system [13], [14]. However, it usually has a non-integer number of ampere turns or different coil radii, which is inconvenient in miniaturized applications.

A saddle coil is a kind of widely used traditional transverse magnetic field coil. Geometrical optimization of a saddle uniform magnetic field coil has been widely studied. The central magnetic field of a saddle coil and its second derivatives were given as functions of the coil geometrical dimensions in a paper by D. M. Ginsberg et al. Also, he solved for the ideal saddle coil structure parameters [15]. However, this ideal saddle coil need a length to diameter ratio of 2. It is difficult to meet the needs of miniature atomic sensors. H. Hanssum developed a method based on the vector potential, in a closed form with elliptic integrals of the first and second kind, to study saddle coils' configurations [16]–[19]. The results were consistent with those from D. M. Ginsberg's work. A configuration of saddle coils was proposed by Seungmun Jeon et al., with the goal of balancing the trade-off between coil height and field uniformity [2]. However, the length to diameter ratio cannot be further reduced, and the uniformity is also compromised. Fourth order Taylor expansions of the magnetic field, which can be used to approximately evaluate the degree of field homogeneity, were derived by F. Bonetto et al. in [4]. Structural parameters for different length to diameter ratios have also been optimized. However, even with these improvements it is still difficult to reach the magnetic field uniformity of an ideal saddle coil. To address the contradiction between the volume and the field uniformity of the saddle coil, we proposed a novel coil structure nested by two pairs of saddle coils in [7]. This design allows us to obtain better magnetic field uniformity for small length to diameter ratios, but its parameter optimization needs further study.

With conventional cylindrical axial coils are difficult to reconcile the conflict between field uniformity and structural simplicity, while with radial coils it is difficult to further reduce volume and improve field uniformity. On the other hand, with the ongoing improvements of in available computing power, coil design methods have made new progress, such as target field methods and different optimization methods. The target field methods has been introduced and explored in many papers [1], [2], [20], [23]. The

application of optimization methods in coil design or magnet design is also very extensive. Practical design of magnetostatic structure using numerical methods was introduced in detail by Wang [24]. Different optimization algorithms were used to calculate the optimal conductor shapes and positions of superconducting shim coils in [25], [26]. Intelligent optimization algorithms have advantages in complex optimization problems, especially when there are multiple peaks or the derivative of the objective function is not continuous. Some researchers have applied intelligent optimization algorithms in coil designs. A genetic algorithm was introduced to design an open high magnetic field MRI superconducting magnet in [27]. A PSO algorithm was introduced to design gradient coil in [28]. Among a variety of intelligent optimization algorithms, the PSO algorithm had achieved good optimization results in many fields because of its good local search ability, good global search ability, and extremely fast convergence speed. In view of this, an uniform magnetic field coil design method is proposed based on the PSO algorithm. Compared with the conventional optimization algorithms, this method has three advantages in the design of a uniform magnetic field coil. First, we can set the necessary constraints, including structural constraints (length to diameter ratio, partial apertures, etc.) and process constraints (line spacing, turns ratio, etc.) in the design. This is more flexible and adaptable than conventional methods. Second, we can solve for higher order uniform magnetic fields. Conventional coil design methods often fail to obtain solutions when solving for coil designs to produce magnetic fields with high-order uniformity. An optimized method can avoid this problem. Third, we can use discrete optimization when optimizing. The discrete optimization used in this paper can avoid the degradation from rounding errors. Parameters with a large number of decimal places are often obtained by the conventional method. There are rounding errors in the application, which degrades the field uniformity. The target field methods can be combined with the boundary element method for designing coils on any type of surface [29]. They can also be used for miniaturized systems that impose stringent manufacturing constraints [30]. The main advantage of the target field method is its simplicity. Coils of different shapes can be obtained by changing the constraints of the current density function. Compared with the target field method, the method we proposed is based on discrete currents, so there is no error caused by current discretization. This method requires the derivation of the analytical expression of the magnetic field and the derivation of its derivative. This process is often complicated and only suitable for coils with relatively simple structures. But from another perspective, a simple structure is also an advantage. The simple structure makes the coil easier to build. In general, the coil design method based on the PSO algorithm and the target field method have their own merits and deserve our further study. At the same time, other new coil design methods are also worthy of attention and research. Based on the PSO algorithm, we designed and processed triaxial cylindrical coils for uniform magnetic fields. Numerical calculations and experimental measurements demonstrate the effectiveness of this method.

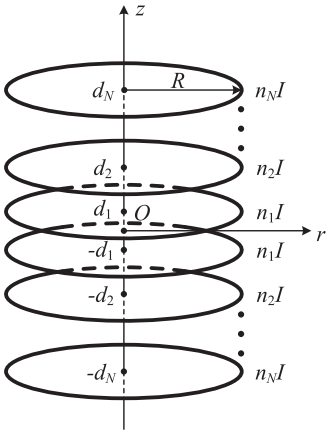

FIGURE 1. General cylindrical axial magnetic field coil structure.

II. METHOD

A. BASIC STRUCTURE OF CYLINDRICAL AXIAL COILS

The general cylindrical axial magnetic field coil structure is shown in Fig. 1. Since the structure is simple and easy to construct, it is very common in practical applications. All circular coils are on the same cylindrical surface and are symmetric about the $z = 0$ plane. The coil structures consist of N pairs of circular coil sets that are symmetric about the $z = 0$ plane. The i-th pair of coil sets are in the $z = \pm d_i$ planes, and each has n_iI ampere-turns. Like previous researchers, we derive the magnetic field on the coil axis and its derivatives at the coil center according to the Biot-Savart law, as in (1). The magnetic field at a point on the coil axis can be expressed by (2).

$$\vec{B} = \frac{\mu_0}{4\pi} \oint \frac{I \mathrm{d}\vec{l} \times \vec{r}}{r^3}. \tag{1}$$

$$\vec{B}|_{(0,0,z)} = \frac{1}{2}\mu_0 I R^2 \sum_{i=1}^{N} n_i \left[R^2 + (z + d_i)^2\right]^{-3/2} \vec{z} + \frac{1}{2}\mu_0 I R^2 \sum_{i=1}^{N} n_i \left[R^2 + (z - d_i)^2\right]^{-3/2} \vec{z}. \tag{2}$$

In the above equations, $\vec{B}|_{(0,0,z)}$ is the magnetic field at a point of coordinates $(0, 0, z)$, $\vec{z}$ is the unit vector in the z direction, $\mu_0 = 4\pi \times 10^{-7}$ H/m is the permeability of free space, I is the current flowing in the coil, R is the coil radius, N is the total number of coil pairs, n_i is the number of turns of the i-th pair of coils, and d_i is the distance between the i-th pair of coils and the $z = 0$ plane.

To simplify the derivation process and represent the similar coils with different radii, all lengths in the coil are expressed as relative values of the radii. Assuming that the coil radius is 1 unit in length, the distance between each pair of coil groups and the $z = 0$ plane is d_i units. When analyzing the magnetic field uniformity, the size of the VOI is expressed in the same form. Derivatives of B_z at the central point along the axis are

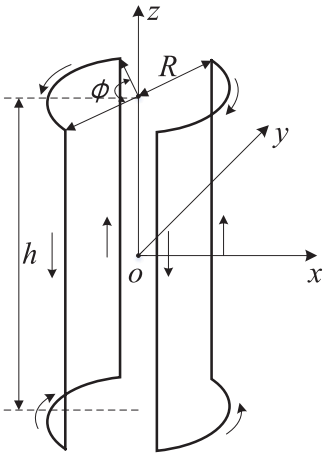

FIGURE 2. General saddle coil structure. The coil structure is composed of four straight segments and four arc segments. In addition to the coil radius R, there are only two independent parameters: the arc angle ϕ and the length to diameter ratio $\alpha = h/2R$.

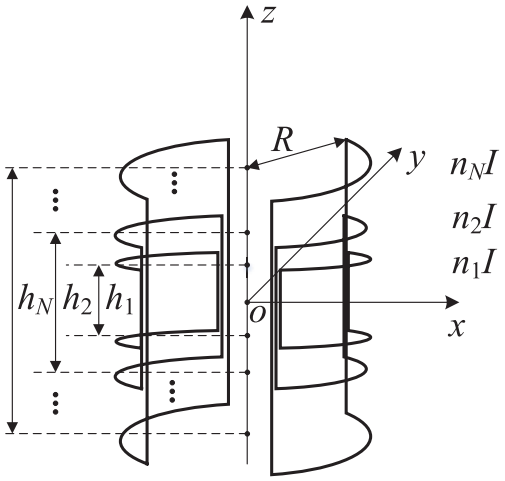

FIGURE 3. Nested saddle coil structure. This coil structure consists of N pairs of saddle coils, each having the same radius but different angles and length to diameter ratio. The i-th pair of saddle coils has an angle ϕ_i, a length to diameter ratio α_i, and its number of ampere turns is n_iI. It is worth mentioning that the directions of currents in the coils are not all the same: some coils have forward current, and some have reverse current.

derived as in (3), as shown at the top of the next page. It is worth mentioning that the odd-order derivatives of B_z at the center point along the axial direction are all zero due to the symmetry of the coil.

B. BASIC STRUCTURE OF CYLINDRICAL RADIAL COILS

A cylindrical coil to produce a radial magnetic field is usually a saddle coil design. The basic saddle coil concept is shown in Fig. 2. However, with this coil structure it is difficult to produce a very uniform magnetic field especially for coils with small length to diameter ratios. In [7], we proposed saddle coil nesting schemes with two nested pairs of coils to improve the uniformity of saddle coils with small length to diameter ratios. In this paper, we extend this approach by nesting N pairs of saddle coils to obtain a more uniform cylindrical radial magnetic field. This extended nested saddle coil structure is shown in Fig. 3. These saddle coils have the same radius but different arc angles and length to diameter ratios.

Similar to axial coils, the center magnetic field of the nested saddle coil and its derivatives were derived, as in (4) and (5), as shown at the top of the next page. For a more complete derivation process and results, see [7].

$$\vec{B}|_{(0,0,0)} = \frac{4\mu_0 I}{\pi D}\sum_{i=1}^{N} n_i\,(s_i-1)^{\frac{1}{2}}(s_i^{-\frac{1}{2}} + s_i^{-\frac{3}{2}})(\sin\frac{\phi_i}{2})\,\vec{i}. \tag{4}$$

In (4), $\vec{i}$ is the unit vector in the x direction, I is the current flowing in the coil, D is the coil diameter, n_i is the number of turns in each pair of saddle coils, h_i and ϕ_i are the height and central angle respectively, and $s_i = 1 + (h_i/D)^2$.

C. APPLICATION OF THE PSO ALGORITHM TO CYLINDRICAL COIL DESIGN

The conventional coil design method uses a Taylor expansion or a ball harmonic expansion at the center of the magnetic field and then solves for the structural parameters of the coil by setting the low-order terms equal to zero. This method is relatively simple for solving for low-order uniform magnetic fields, but when designing higher-order coils for uniform magnetic fields, it often happens that the equations have no solution. Even if solutions are obtained, the ampere-turns are usually not integers, which may cause the coil structure to be too complicated for practical applications. Also, with this method it is difficult to set the necessary constraints (such as length to diameter ratio, volume, etc.) when solving for parameters according to an application's requirements. Therefore, we use optimization method instead of solving the equations to obtain the coil structure parameters. This optimization method can make up for the problems of the conventional coil design method.

The PSO algorithm is an intelligent optimization algorithm proposed by Eberhart and Kennedy in 1995, based on the bird social behavior model developed by the biologist Frank Heppner [31]. Birds and fish adjust their physical movement to avoid predators, seek food and mates, and optimize their environmental variables such as temperature, etc. Each particle adjusts its flight according to its own experience and its companions' experience. This optimization algorithm has been successfully applied in many fields. Each individual is called a "particle," which represents a potential solution to a problem [32]. As described in [32], the standard particle swarm optimization algorithm can be represented by the following model. In a D-dimensional space, the position of the i-th particle can be expressed as $X_i = (x_{i1}, x_{i2}, ..., x_{iD})$. The best previous position (the position giving the best fitness value) of any particle is recorded and represented as $P_i = (p_{i1}, p_{i2}, ..., p_{iD})$. The index of the best particle among all the particles in the population is represented by the symbol g. The rate of change of the position (velocity) for particle i is represented as $V_i = (v_{il}, v_{i2}, ..., v_{iD})$. The particles are

$$
\begin{aligned}
\left.\frac{\partial^2 B_z}{\partial z^2}\right|_{(0,0,0)} &= 3\mu_0 I \sum_{i=1}^{N} n_i \frac{4d_i^2 - 1}{\left(1 + d_i^2\right)^{7/2}} \\
0 \left.\frac{\partial^4 B_z}{\partial z^4}\right|_{(0,0,0)} &= 45\mu_0 I \sum_{i=1}^{N} n_i \frac{8d_i^4 - 12d_i^2 + 1}{\left(1 + d_i^2\right)^{11/2}} \\
\left.\frac{\partial^6 B_z}{\partial z^6}\right|_{(0,0,0)} &= 315\mu_0 I \sum_{i=1}^{N} n_i \frac{64d_i^6 - 240d_i^4 + 120d_i^2 - 5}{\left(1 + d_i^2\right)^{15/2}} \\
\left.\frac{\partial^8 B_z}{\partial z^8}\right|_{(0,0,0)} &= 14175\mu_0 I \sum_{i=1}^{N} n_i \frac{128d_i^8 - 896d_i^6 + 1120d_i^4 - 280d_i^2 + 7}{\left(1 + d_i^2\right)^{19/2}} \\
\left.\frac{\partial^{10} B_z}{\partial z^{10}}\right|_{(0,0,0)} &= 467775\mu_0 I \sum_{i=1}^{N} n_i \frac{512d_i^{10} - 5760d_i^8 + 13440d_i^6 - 8400d_i^4 + 1260d_i^2 - 21}{\left(1 + d_i^2\right)^{23/2}} \\
\left.\frac{\partial^k B_z}{\partial z^k}\right|_{(0,0,0)} &= 0(k = 1, 3, 5...).
\end{aligned} \tag{3}
$$

$$
\begin{aligned}
\left.\frac{\partial^2 B_x}{\partial x^2}\right|_{(0,0,0)} &= \frac{16\mu_0 I}{\pi D^3} \sum_{i=1}^{N} n_i {s_i}^{-\frac{7}{2}} (s_i - 1)^{\frac{1}{2}} (\sin\frac{\phi_i}{2}) \cdot \left[-(8{s_i}^3 + 4{s_i}^2 + 3s_i + 5)\sin^2\frac{\phi_i}{2} + 6{s_i}^3 + 3{s_i}^2 + 15 \right] \\
\left.\frac{\partial^2 B_x}{\partial y^2}\right|_{(0,0,0)} &= \frac{16\mu_0 I}{\pi D^3} \sum_{i=1}^{N} n_i {s_i}^{-\frac{7}{2}} (s_i - 1)^{\frac{1}{2}} (\sin\frac{\phi_i}{2}) \cdot \left[(8{s_i}^3 + 4{s_i}^2 + 3s_i + 5)\sin^2\frac{\phi_i}{2} - (6{s_i}^3 + 3{s_i}^2 + 3s_i) \right] \\
\left.\frac{\partial^2 B_x}{\partial z^2}\right|_{(0,0,0)} &= \frac{16\mu_0 I}{\pi D^3} \sum_{i=1}^{N} n_i {s_i}^{-\frac{7}{2}} (s_i - 1)^{\frac{1}{2}} (3s_i - 15) \sin\frac{\phi_i}{2}.
\end{aligned} \tag{5}
$$

manipulated according to (6).

$$
\begin{aligned}
v_{id}(k) &= \omega \cdot v_{id}(k-1) + c_1 \cdot \text{rand}(\,) \cdot (p_{id} - x_{id}(k-1)) \\
&\quad + c_2 \cdot \text{Rand}(\,) \cdot (p_{gd} - x_{id}(k-1)) \\
x_{id}(k) &= x_{id}(k-1) + v_{id}(k) \; (k = 1, 2, 3 \cdots).
\end{aligned} \tag{6}
$$

where k is the current number of iterations, ω is the inertia weight, c_1 and c_2 are acceleration constants, and rand( ) and Rand( ) are two random functions which both have a range of [0, 1]. The velocity of particle i has three parts. The first part is the ''inertial'' part, which represents the inertia of the previous behavior of the particles. The second part is the ''cognition'' part, which represents the private thinking of the particle itself. The third part is the ''social'' part, which represents the collaboration among the particles. It should be noted that ω, c_1, and c_2 do not have to be constant values, and can be adjusted according to the number of iterations. A variety of improved particle swarm optimization algorithms have also been derived. The PSO algorithm is simpler than a genetic algorithm. It does not have the ''crossover'' and ''mutation'' operations of a genetic algorithm. It searches for the global optimal by following the current best value. This algorithm's advantages include easy implementation, high precision, fast convergence. Also, the particle swarm algorithm is a parallel algorithm.

In order to apply the PSO algorithm, we transform the design of a uniform magnetic field coil into an optimization problem. Taking the design of the cylindrical axial coil as an example, the position of each circular coil pair ($d = (d_1, d_2, ..., d_N)$) is optimized as a particle swarm problem. The absolute value of each derivative of the coil center in the axial direction is used as the fitness value as a criterion for evaluating the ''goodness'' of the particle position. This multi-objective optimization is transformed into a single-objective optimization by a weighted sum. In addition, a relative position constraint is set by a penalty function. This allows the spacing between coils to be constrained to accommodate certain machining accuracy and opening limitations. For example, in atomic sensors, the center of the coil typically has an aperture to admit light. It is worth mentioning that the ampere-turns ratio of each coil is designed to be 1 to facilitate processing and manufacturing. Optimization of the cylindrical axial coil can be expressed in a mathematical form as (7).

$$
\begin{aligned}
&\text{Min} \sum_{k=1}^{k_p} \omega_k \cdot \left| \left.\frac{\partial^{2k} B_z}{\partial z^{2k}}\right|_{(0,0,0)} \right| \\
&\text{s.t. } d_{i+1} - d_i \geq ds_{\min} (i = 1, 2, ..., N-1) \\
&\quad d_{\min \leq} d_i \leq d_{\max} (i = 1, 2, ..., N).
\end{aligned} \tag{7}
$$

TABLE 1. Parameters of the barker four-coil.

Barker Four-Coil	
$d_1 = (0.243186...)R$	$n_1 I_1 = 0.442391...$
$d_2 = (0.940731...)R$	$n_2 I_2 = 1$

In (7), k_p is the number of terms of the low-order derivative to be optimized, N is the number of terms of the low-order derivative to be optimized, ω_k is the weight of each derivative in the objective function, $d = [d_1, d_2..., d_N]$ is the position of each pair of coils, ds_{min} is the minimum coil spacing requirement that is limited by the manufacturing process, and d_{max} and d_{min} are the maximum and minimum limits of the coil position. The parameter d_{max} is limited by coil's length to diameter ratio. Since atomic sensors typically have holes in the center of the coil to allow light to pass through the required gas cell, d_{min} is often limited by the size of the opening in the center of the coil. Compared to the conventional method of solving equations, setting these constraints increases our controllability of the parameters of the coil's structure. When using the conventional method for coil design, we can only passively accept the solution results. However, sometimes these results do not satisfy our structure. This problem does not occur with our design method.

In our design, the parameter N determines the upper limit of the coil uniformity, and the parameter k_p determines the degree of optimization of the coil within this upper limit. By using larger N and k_p, we can easily obtain a coil to produce a magnetic field with higher-order uniformity. This is another advantage of this method over traditional coil design methods. In this paper, we set the values of both N and k_p to be 8. That is to say, we use 8 pairs of circular coil pairs as the basic structure of the coil, and optimize the lowest 8 even-order derivatives as the objective function. The Barker four-coil, designed using the conventional coil design method, only utilizes the lowest 3 even-order derivatives. This allows us to design coils with a more uniform magnetic field than coils designed by conventional coil methods.

The coil parameters obtained by conventional methods are usually infinite decimals. Taking the Barker four-coil as an example, the position of the two pairs of coils and the turns ratio of the coils are all perfectly precise decimals. Its parameters are shown in Table 1. In actual machining, we must round off these parameters according to the machining accuracy. This rounding error will degrade the uniformity of the magnetic field. In this paper, the proper preprocessing is carried out using the PSO algorithm, which avoids the rounding errors of the coil positions. Since the PSO algorithm is based on a random search, its search is continuous. Before calculating the fitness values of the particles in each iteration, we first round the particle positions. This allows us to perform discrete optimizations.

Since the PSO algorithm is a random search algorithm, the initial values of the population are also randomly selected within the defined interval which is dependent on the coil structure. In order to use the parallel computing power of the computer to find the optimal value faster, a larger population and fewer iterations have been selected. In the case of a population of 4,000,000 and a number of iterations of 400, the running time is about 4 hours. After the above PSO algorithm, we can obtain an axial coil for the high-order field uniformity that we expect. The same method can be applied to the design of radial coils. A highly uniform radial magnetic field is obtained by optimizing parameters such as the arc angle and the length to diameter ratio of each nested saddle coil.

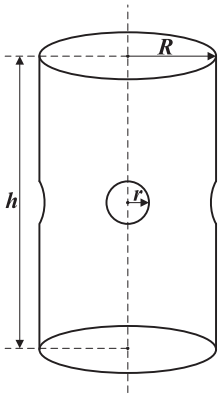

FIGURE 4. Atomic sensor requirements for the opening of a triaxial cylindrical magnetic field coil.

III. NUMERICAL RESULTS

Using the method described in Section II, the desired optimal coil structure can be obtained. In order to eliminate the effect of different coil radii on the evaluation of the target field uniformity, all lengths are measured in terms of the coil radii. This will not affect our evaluation results of the magnetic field uniformity. Due to the large volume of existing magnetic field sensors, it is difficult to measure the magnetic fields at different locations directly in coils with smaller radii. Coils with a large radius (63mm) were used for numerical calculations and experiments. Here, a cylindrical coil design with a radius of 63 mm and a length to diameter ratio of 1.75 is taken as an example. As shown in Fig. 4, there are four openings on the cylindrical surface of the coil, each with a radius of 9 mm. Also, the wire spacing is also constrained according to the actual process requirements. With these structural and process constraints we designed an axial coil for a uniform magnetic field, composed of 8 pairs of circular coil pairs and a radial uniform magnetic field coil composed of 6 pairs of saddle coils. The optimized structural parameters are shown in Table 2. Similar to the discussion in Section II, these structural parameters are also expressed in terms of the relative size of the coil's radius.

To verify the effectiveness of the optimization, we performed numerical calculations on the designed coils. The integerized Lee-Whiting coil mentioned in [11] and the balanced single saddle coil mentioned in [2] were used as a reference set. Coils obtained by the genetic algorithm were used as another reference set. For fairness, the coils' parameters

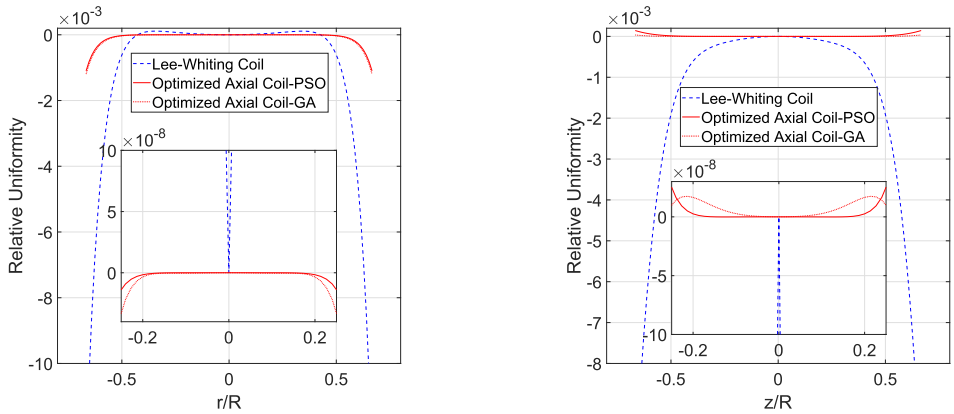

FIGURE 5. The relative magnetic field errors of the three axial coil along the r and z axes. (a) shows the magnetic field error distribution along the radial axis of the Lee-Whiting coil, the axial coil optimized by PSO, and the axial coil optimized by GA. (b) shows the same errors along the axial axis. The axial coil optimized by PSO has better magnetic field uniformity than the Lee-Whiting coil, whether over a wide or a narrow range. Especially in the range $[-0.25R, 0.25R]$, the magnetic field uniformity performance is improved by about 4 orders of magnitude. Moreover, the performance of the coil obtained by PSO is better than that obtained by GA.

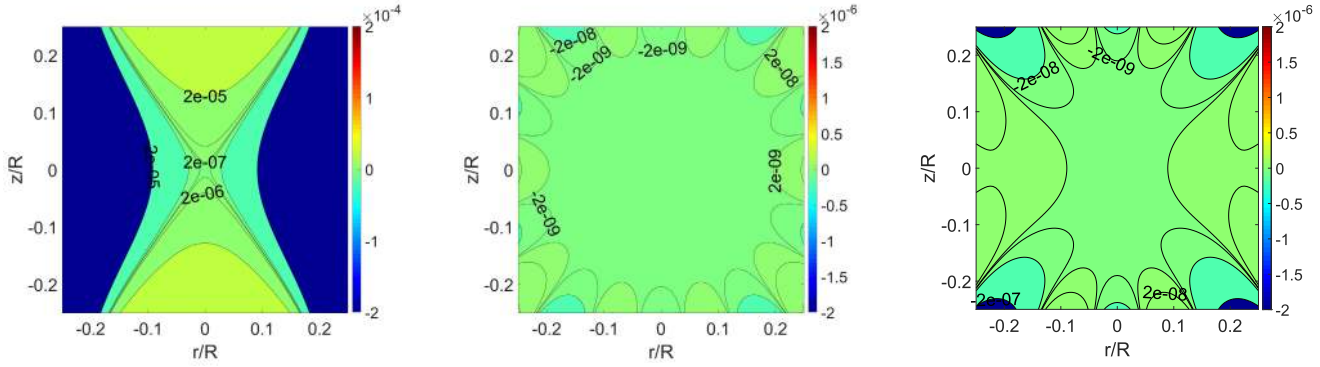

FIGURE 6. The magnetic field error distribution of the two axial coils on the $r-z$ plane, showing the magnetic field error distribution for a cylinder at the center of the coil with a radius of $0.25R$ and a height of $0.5R$. (a) The magnetic field error distribution for a Lee-Whiting coil, (b) the magnetic field error distribution for the axial coil optimized by PSO, and (c) the magnetic field error distribution for the axial coil optimized by GA. The magnetic field error of the axial coil optimized by PSO is decreased by about 4 orders of magnitude compared to the Lee-Whiting coil.

TABLE 2. The optimized structural parameters of triaxial cylindrical magnetic field coils using particle swarm optimization.

Axial Coil		Radial Coil		
$d_1 = 0.1504R$	$n_1 = 1$	$h_1 = 0.4333R$	$\phi_1 = 20.000°$	$n_1 = 1$
$d_2 = 0.4539R$	$n_2 = 1$	$h_2 = 0.9293R$	$\phi_2 = 23.026°$	$n_2 = -1$
$d_3 = 0.7514R$	$n_3 = 1$	$h_3 = 3.0517R$	$\phi_3 = 47.250°$	$n_3 = 1$
$d_4 = 1.0361R$	$n_4 = 1$	$h_4 = 3.4393R$	$\phi_4 = 96.732°$	$n_4 = 1$
$d_5 = 1.4832R$	$n_5 = 1$	$h_5 = 3.4700R$	$\phi_5 = 136.670°$	$n_5 = 1$
$d_6 = 1.6378R$	$n_6 = 1$	$h_6 = 3.5000R$	$\phi_6 = 160.000°$	$n_6 = 1$
$d_7 = 1.6926R$	$n_7 = 1$			
$d_8 = 1.7297R$	$n_8 = 1$			

TABLE 3. The optimized structural parameters of triaxial cylindrical magnetic field coils using genetic algorithm.

Axial Coil		Radial Coil		
$d_1 = 0.1506R$	$n_1 = 1$	$h_1 = 0.4312R$	$\phi_1 = 32.702°$	$n_1 = 1$
$d_2 = 0.4521R$	$n_2 = 1$	$h_2 = 0.8629R$	$\phi_2 = 36.460°$	$n_2 = -1$
$d_3 = 0.7541R$	$n_3 = 1$	$h_3 = 2.4732R$	$\phi_3 = 42.780°$	$n_3 = 1$
$d_4 = 1.0281R$	$n_4 = 1$	$h_4 = 3.4360R$	$\phi_4 = 94.148°$	$n_4 = 1$
$d_5 = 1.4694R$	$n_5 = 1$	$h_5 = 3.4662R$	$\phi_5 = 138.126°$	$n_5 = 1$
$d_6 = 1.6515R$	$n_6 = 1$	$h_6 = 3.4981R$	$\phi_6 = 154.404°$	$n_6 = 1$
$d_7 = 1.6942R$	$n_7 = 1$			
$d_8 = 1.7300R$	$n_8 = 1$			

were obtained using the GA under the same criteria (number of loops, etc.). The coils' parameters obtained by the GA are shown in Table 3. Magnetic field produced by these six coils are shown visually by the following figures. In these figures, all dimensions are also expressed as relative values of the radius.

We first analyzed the relative errors of the magnetic fields produced by the axial coils. In Fig. 5, (a) shows the magnetic field error distribution along the axial axis of the Lee-Whiting coil, the axial coil optimized by PSO, and the axial coil optimized by GA. (b) shows that along the radial axis. It should be noted that since the three axial coils are symmetric in all

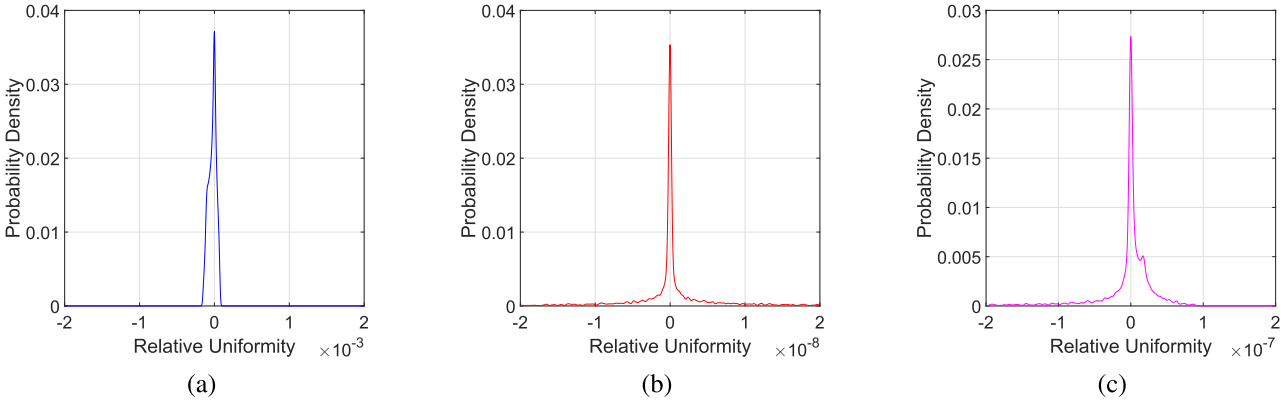

FIGURE 7. The probability distribution curves of the magnetic field relative error for the three axial coils. The relative errors of all points in the entire target region are considered as probability samples. This figure shows the magnetic field relative error probability density distribution in a cylindrical volume with a radius of $0.25R$ and a height of $0.5R$. (a) shows the magnetic field relative error probability density distribution of Lee-Whiting coil, (b) shows that of the axial coil optimized by PSO, and (c) shows that of the axial coil optimized by GA. The figure shows that within the target volume, the relative error of the magnetic field produced by the Lee-Whiting coil is on the order of 10^{-4}, while the relative error of the magnetic field produced by the axial coil optimized by PSO is on the order of 10^{-9}.

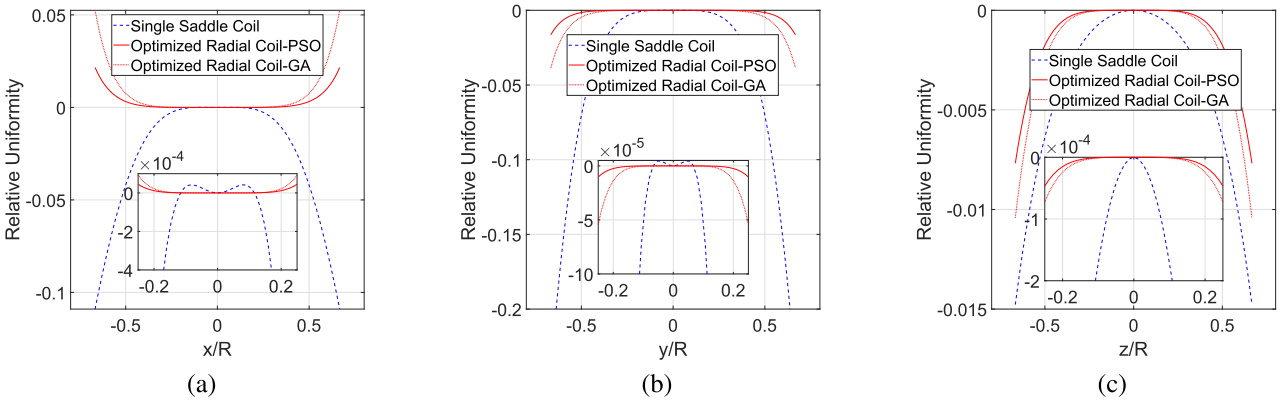

FIGURE 8. The magnetic field relative errors of the three radial coils along the x, y, and z axes. (a), (b), and (c), respectively, show the magnetic field error distributions of the saddle coil and optimized radial coil along its three coordinate axes. The radial coil optimized by PSO has better magnetic field uniformity than saddle coil, whether over a wide or a narrow range. Especially in the range of $[-0.25R, 0.25R]$, the magnetic field error of the radial coil optimized by PSO is decreased by about 2 orders of magnitude compared the saddle coil.

radial directions, the magnetic field model can be reduced from 3-D models to 2-D models without any loss of information. Therefore, the magnetic field of the axial coil is calculated in the $r-z$ coordinate system. In this case, the range of $[-0.67R, 0.67R]$ on the coordinate axis is the analyzed interval. The magnetic field relative error in the range of $[-0.25R, 0.25R]$ on the coordinate axis is shown in detail. In Fig. 6, (a), (b) and (c) show the magnetic field error distribution in the $r-z$ plane of the three axial coils, respectively. This figure shows the magnetic field error distribution of a cylinder at the center of the coil with a radius of $0.25R$ and a height of $0.5R$. We introduce the probability distribution curve of the magnetic field relative error in the VOI to reflect the magnetic field uniformity of the coils in [7]. The relative errors at all points in the entire target region are considered as probability samples. In Fig. 7, (a), (b) and (c) show the probability distribution curves of the magnetic field relative errors of the three axial coils. Similarly, this figure shows the magnetic field relative error probability density distribution in a cylindrical at the center of the coil with a radius of $0.25R$ and a height of $0.5R$.

Similarly, we also analyzed the magnetic field uniformity of the three radial coils from these three points of view. In Fig. 8, (a), (b), and (c) show the magnetic field relative errors along three coordinate axes of the saddle coil, the axial coil optimized by PSO, and the axial coil optimized by GA, respectively. In Fig. 9 (a), (b), and (c) show the magnetic field relative error distribution of saddle coil on the three coordinate planes, while (d), (e), and (f) show that of the the axial coil optimized by PSO, (g), (h), and (i) show that of the the axial coil optimized by GA. In Fig. 10, (a), (b) and (c) show the probability distribution curves of the magnetic field relative error of the radial coils respectively. This analysis is very necessary for radial coils, considering that it can

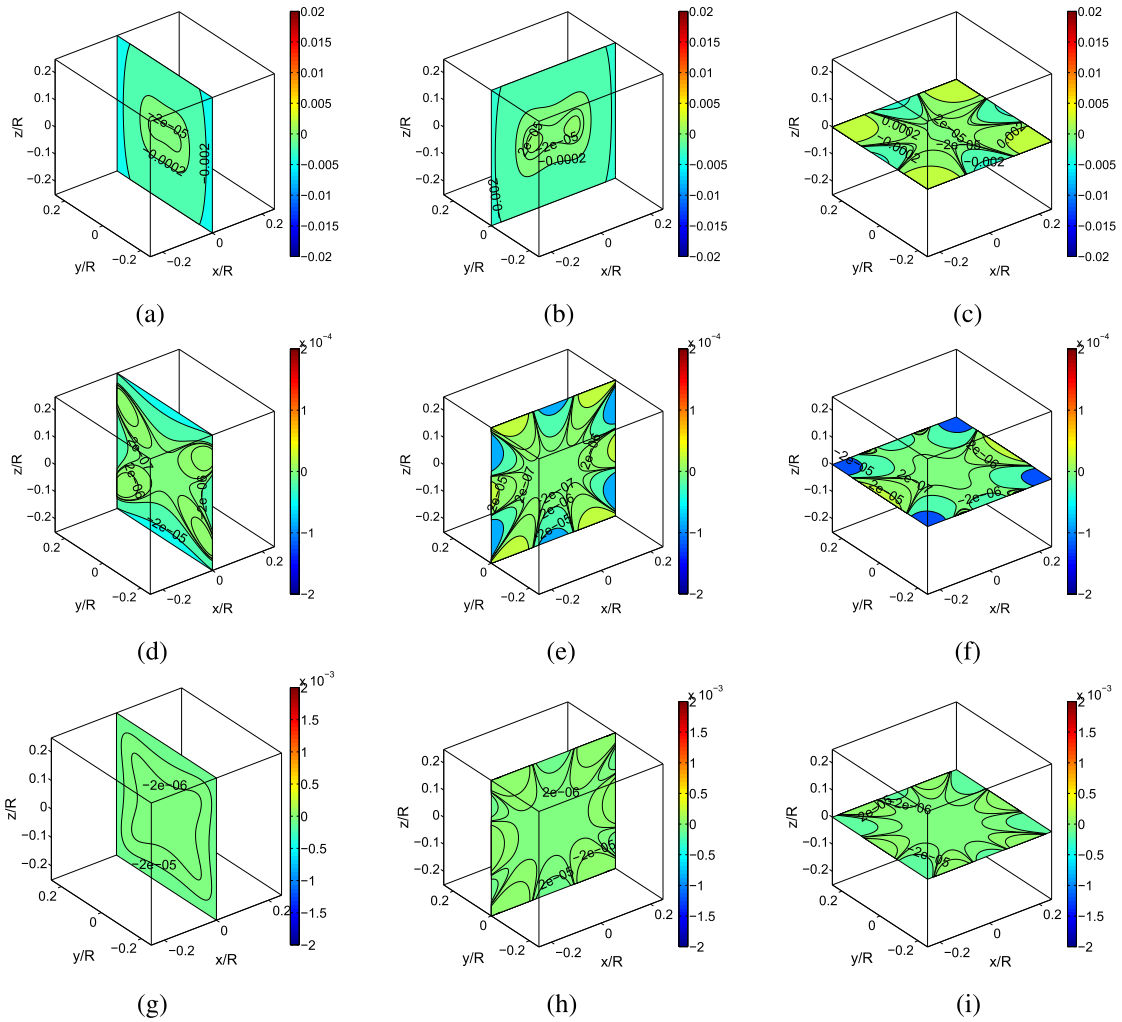

FIGURE 9. The magnetic field error distribution of the two radial coils on three coordinate planes, showing the magnetic field error distribution in the center of the coordinate plane with a side length of 0.5R. (a), (b), and (c) show the magnetic field error distribution for a saddle coil. (d), (e), and (f) show that of the radial coil optimized by PSO. (g), (h), and (i) show that of the radial coil optimized by GA. The magnetic field uniformity performance of the radial coil optimized by PSO is improved by about 2 orders of magnitude compared the saddle coil.

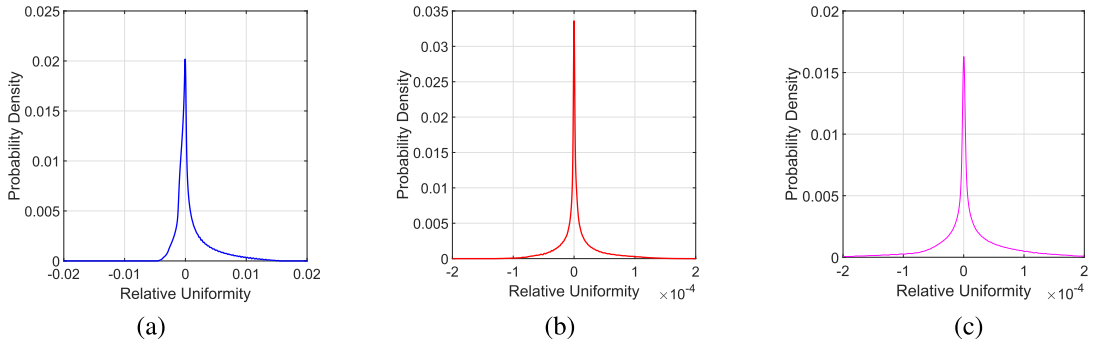

FIGURE 10. The probability distribution curves of the magnetic field relative errors of the three radial coils. This figure shows the magnetic field relative error probability density distribution in a cube with a side length of 0.5R. (a) shows the magnetic field relative error probability density distribution for saddle coils, (b) the radial coil optimized by PSO, and (c) the radial coil optimized by GA. The figure shows that within the target volume, the relative error of the magnetic field of saddle coils is on the order of 10^{-3}, while the relative error of the magnetic field of the radial coil optimized by PSO is on the order of 10^{-5}.

reflect the field uniformity in the whole VOI. Unlike the axial coils, in the three figures the VOI is changed from a cylinder with a radius of 0.25R and a height of 0.5R to a cube having sides with lengths of 0.5R.

It can be seen from the above numerical analysis that the axial coil geometry obtained using the PSO algorithm has a magnetic field uniformity about 4 orders of magnitude better than that of the Lee-Whiting coil. The radial coil obtained via the PSO algorithm has a magnetic field uniformity that is 2 orders of magnitude better than that of the saddle coil. These results are very useful for most applications requiring uniform magnetic fields. At the same time, it can be seen that the uniformity of the magnetic field of the coil obtained by the PSO is slightly better than that obtained by the GA.

IV. EXPERIMENTAL RESULTS AND DISCUSSION

In order to experimentally verify the effectiveness of the coil design method using the PSO algorithm, the optimized axial and radial coils with a radius of 63 mm were manufactured by Flexible Printed Circuit (FPC) technology. The flexible coils were glued to the surface of a cylindrical frame and tested with a flux-gate magnetometer. The axial and radial coils are driven by two independent current sources. The individual loops of the axial coil are connected in series. The various parts of the radial coil are also connected in series. In order to eliminate the effect of the connecting lines on the uniformity of the target field, the currents flowing into and out of the connecting lines are opposite in direction. The magnetic induction at different points on the coordinate axis was measured with the flux-gate magnetometer. The radial coil designed by the PSO algorithm has a magnetic field uniformity of 10^{-6} in a cube with a side length of $0.4R$ at the center of the coil. The magnetic field uniformity can reach 10^{-9} for axial coil. This exceeded the resolution of most current magnetic field sensors. Therefore, we measured the magnetic field distribution over a wide range along the coordinate axis. This can also verify the effectiveness of the design method. For convenient testing, the magnetic field was measured over the range of $[-0.67R, 0.67R]$ along the coordinate axis of the coil magnetic field.

In order to suppress the influence of environmental magnetic field fluctuations, we used alternating current to drive the coil and measure the amplitude of the alternating magnetic field. The LDC 205C a Thorlabs current source which can supply up to 500 mA current, was selected as the drive current source for the coils. The current source has a time drift of less than 10 uA per day and a temperature drift of less than 50 ppm/°C. It should be noted that this current source was modulated by a single-frequency sinusoidal voltage signal. A Mag-03 flux-gate magnetometer from Bartington Instruments, which has a measuring range of ± 100 μT and a low noise below 6 pTrms/Hz$^{1/2}$ at1 Hz, was used as the magnetic field sensor. The MF LI Lock-in Amplifier produced by Zurich Instruments was used as a demodulator to accurately obtain the amplitude of the alternating magnetic field. Considering the bandwidth of the Mag-03 and the noise power spectrum of the ambient noise, a sinusoidal current with a magnitude of 200 mA and a frequency of 20 Hz was applied to the coil. Then, the magnetic field signal measured by the Mag-03 was demodulated with MF LI to obtain the amplitude of the magnetic field. The schematic diagram of the measurement system and the actual field test are shown in Fig.11.

TABLE 4. Magnetic field measurements of the two coils along the magnetic field axis.

Axial Coil			Radial Coil		
z(mm)	z/R	B_z(nT)	x(mm)	x/R	B_x(nT)
-42.5	-0.674	12149.210±0.252	-40	-0.634	8281.202±0.209
-37.5	-0.594	12146.712±0.455	-35	-0.555	8221.391±0.143
-32.5	-0.515	12146.238±0.200	-30	-0.475	8182.427±0.140
-27.5	-0.436	12145.454±0.237	-25	-0.396	8166.752±0.142
-22.5	-0.357	12144.761±0.162	-20	-0.317	8159.332±0.136
-17.5	-0.277	12144.959±0.247	-15	-0.238	8155.395±0.154
-12.5	-0.198	12145.298±0.200	-10	-0.158	8153.274±0.137
-7.5	-0.119	12145.134±0.210	-5	-0.079	8151.629±0.151
-2.5	-0.040	12145.680±0.180	0	0	8150.766±0.147
2.5	-0.040	12145.656±0.232	5	0.079	8150.777±0.133
7.5	0.119	12145.051±0.233	10	0.158	8150.872±0.213
12.5	0.198	12145.094±0.236	15	0.238	8152.274±0.195
17.5	0.277	12145.321±0.205	20	0.317	8155.489±0.232
22.5	0.357	12145.257±0.205	25	0.396	8162.564±0.198
27.5	0.436	12144.724±0.280	30	0.475	8177.006±0.367
32.5	0.515	12145.693±0.208	35	0.554	8208.963±0.150
37.5	0.594	12146.367±0.382	40	0.634	8282.192±0.122
42.5	0.674	12149.111±0.226			

TABLE 5. The coil constant measurements for the two coils.

Axial Coil		Radial Coil	
I(mA)	B_{z0}(nT)	I(mA)	B_{x0}(nT)
0	0.122±0.062	0	0.129±0.065
25	1519.065±0.118	25	1019.296±0.104
50	3037.656±0.102	50	2038.157±0.101
75	4554.064±0.129	75	3057.265±0.102
100	6071.739±0.127	100	4075.753±0.105
125	7590.282±0.190	125	5094.287±0.122
150	9108.342±0.143	150	6113.086±0.116
175	10626.348±0.200	175	7132.231±0.163
200	12144.538±0.273	200	8150.997±0.161

While testing the magnetic field distribution along the coordinate axis, we also tested the coil constant at the center of the coil. The measurements of the two coils are shown in Fig.12. Tables 4 and 5 give the complete data along with its uncertainties.

By analyzing these measurements, there are two points to discuss. First, we found that the measured values were slightly smaller than the theoretical values. This may be caused by the gain reduction of the magnetometer. Second, the magnetic field distribution along the coordinate axis is basically consistent with the theoretical curve, but we cannot deny that there were still some small deviations between the measured and theoretical results. This may be due to insufficient sensor resolution and spatial resolution (especially for axial coils), current source noise, and inadequate positioning accuracy. In particular, the flux-gate magnetometer does not measure the magnetic field at one point but measures the macroscopic magnetic field through a small volume. That is to say its spatial resolution is insufficient. In addition, there may be some errors in the coil fabrication, which also affects the distribution of the magnetic field. Despite this, the coils

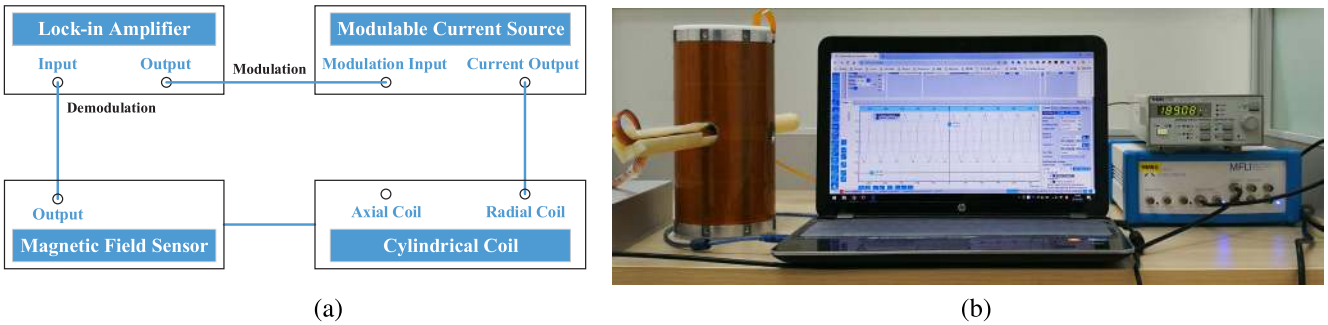

FIGURE 11. The schematic diagram of the test system. (a) shows the schematic of the measurement system. With using DC measurements, changes of the magnetic field with position are completely masked by environmental magnetic field fluctuations. Therefore, a modulation and demodulation approach was used to avoid susceptibility to errors due to fluctuations in the environmental magnetic field. (b) shows the instrument used in the test.

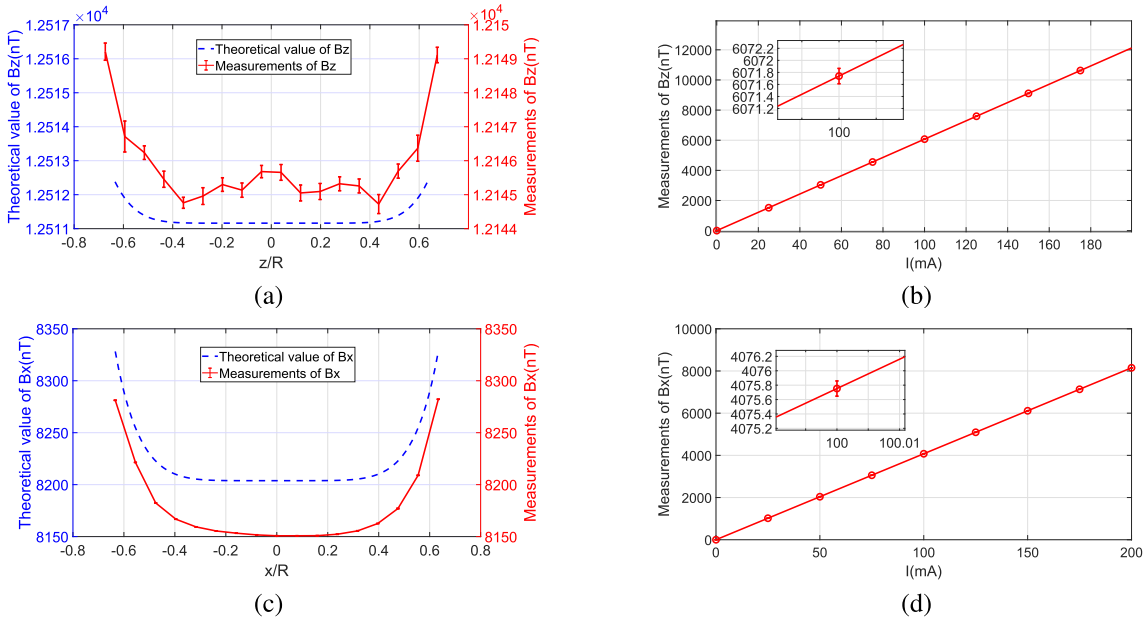

FIGURE 12. The measurements of the two optimized coils. (a) and (c) respectively show the magnetic field measurements for the axial and radial coils along the magnetic field axis with the range of $[-0.67R, 0.67R]$. The measured results for the two optimized coils are satisfactory considering factors such as coil fabrication tolerances, measurement errors, and the sensor's spatial resolution. (b) and (d) show the coil constant measurements for the axial and radial coils, respectively. Through a curve fitting calculation, we found the coil constant of the axial coil was 60.718 nT/mA with a RMSE value of 0.599 nT/mA. For a reference, the theoretical calculated value was 62.556 nT/mA. The coil constant of the radial coil was 40.753 nT/mA with a RMSE value of 0.230 nT/mA. The theoretical calculated value was 41.019 nT/mA. The actual measurement results are slightly smaller than the theoretical value, which may be related to factors such as the gain attenuation of the sensor. Overall, the measurements are quite satisfactory.

we designed still have satisfactory magnetic field uniformity. In particular, when the axial coil has a center magnetic field of 12145.5 nT, even with measurement errors the magnetic field has a variation of only 1.5 nT within the $\pm 0.5R$ range. This means that the magnetic field uniformity within the range of $\pm 0.5R$ reaches 1.2×10^{-4}, which is a very satisfactory result. This uniformity is roughly equivalent to the theoretical uniformity of a Lee-Whiting coil over the $\pm 0.2R$ range. Therefore, this coil design method not only improves the uniformity of the coil magnetic field, but also provides the possibility of miniaturization of the coil, especially considering that each coil has the same number of ampere-turns. However, we cannot ignore the difference between the experimental value and the theoretical value. Impurities brought about by machining error and environmental factors can both cause considerable degradation in field quality. Nevertheless, it is still meaningful to explore the design method of coils with superior field uniformity. At least, it should be ensured that our coil design method is not the factor limiting the field uniformity. So, once a better environment and more precise manufacturing process can be provided, a superior field uniformity can be realized. Of course, the significance of this research is that it gives us the possibility to reduce the coil volume for the same VOI and uniformity requirements. Taking the machining error of an axial coil into consideration, it may be difficult to achieve a field uniformity of 1 ppb in the

small center of the center (within the center $\pm 0.2R$ volume). However, as for the large center of the center (within the center $\pm 0.5R$ volume), an uniformity of several tens of ppm can be obtained with the scheme proposed in this paper. For the original coil scheme, the field uniformity can only be achieved within a volume of $\pm 0.2R$ in the center. This means that our coil can provide the same VOI with a smaller volume occupation. This is beneficial for sensor miniaturization. In NMR, field homogeneity is usually improved/maintained by shimming, either using passive elements or active coils, which is typically based on spherical harmonics. Shimming is also an effective way to improve the magnetic field uniformity in miniature atomic sensors. Because of the flexibility of the active coils, it was chosen to achieved field homogeneity in miniature atomic sensors. This not only compensates for the degradation of the magnetic field uniformity caused by manufacturing tolerances, but also compensates for the harmonic components of the magnetic field that exist in the environmental magnetic field itself. Since the available space of the miniature atomic sensor is constrained, only the primary and secondary spherical harmonic components will be considered. This deserves our further design.

V. CONCLUSION

An innovative design method for highly uniform magnetic field coils based on the PSO algorithm is proposed in this paper. This method can address the problem in the design of a magnetic field with high order uniformity, especially for the constraints seen with miniature atomic sensors. It also provides the possibility of miniaturization of the coil for a specific VOI size, making it an excellent choice for miniaturized applications. Theoretical calculations and experimental measurements prove that it is a very effective design method for coils that need to produce highly uniform magnetic fields. More importantly, this coil design method can also be used to design gradient field coils or other shaped coils. We also designed an axial gradient coil which has a larger linear region than a conventional gradient coil, although that work is not covered in this paper. The intelligent optimization algorithms represented by PSO algorithms have unique advantages and great potential for coil design. The applications of these algorithms in coil design deserve further explorations.

REFERENCES

[1] K. F. Smith, N. Crampin, J. M. Pendlebury, D. J. Richardson, D. Shiers, K. Green, A. I. Kilvington, J. Moir, H. B. Prosper, D. Thompson, N. F. Ramsey, B. R. Heckel, S. K. Lamoreaux, P. Ageron, W. Mampe, and A. Steyerl, "A search for the electric dipole moment of the neutron," *Phys. Lett. B*, vol. 234, nos. 1–2, pp. 191–196, 1990.

[2] S. Jeon, G. Jang, H. Choi, and S. Park, "Magnetic navigation system with gradient and uniform saddle coils for the wireless manipulation of micro-robots in human blood vessels," *IEEE Trans. Magn.*, vol. 46, no. 6, pp. 1943–1946, Jun. 2010.

[3] M. Tsuchimoto, K. Demachi, and I. Itoh, "Numerical evaluation of uniform magnetic field within superconducting swiss roll," *Phys. C, Supercond.*, vols. 412–414, pp. 719–722, Oct. 2004.

[4] F. Bonetto, E. Anoardo, and M. Polello, "Saddle coils for uniform static magnetic field generation in NMR experiments," *Concepts Magn. Reson. B, Magn. Reson. Eng.*, vol. 29B, no. 1, pp. 9–19, 2006.

[5] E. J. Eklund, "Microgyroscope based on spin-polarized nuclei," Tech. Rep., 2008.

[6] H. Zhang, S. Zou, and X. Chen, "Ingenious method for measuring the non-orthogonal angle of the saddle-shaped coils of an SERF atomic magnetometer system," *IEEE Trans. Magn.*, vol. 52, no. 10, Oct. 2016, Art. no. 4002906.

[7] W. Wu, B. Zhou, G. Liu, L. Chen, J. Wang, and J. Fang, "Novel nested saddle coils used in miniature atomic sensors," *AIP Adv.*, vol. 8, no. 7, 2018, Art. no. 075126.

[8] M. W. Garrett, "Thick cylindrical coil systems for strong magnetic fields with field or gradient homogeneities of the 6th to 20th order," *J. Appl. Phys.*, vol. 38, no. 6, pp. 2563–2586, 2004.

[9] J. R. Barker, "New coil systems for the production of uniform magnetic fields," *J. Sci. Instrum.*, vol. 26, no. 8, pp. 273–275, 1949.

[10] G. E. Lee-Whiting, "Uniform magnetic fields," At. Energy Project Canada, ChalkRiver Project Res. Develop., Ottawa, ON, Canada, Tech. Rep. CRT-673, 1957, p. 28.

[11] J. L. Kirschvink, "Uniform magnetic fields and double-wrapped coil systems: Improved techniques for the design of bioelectromagnetic experiments," *Bioelectromagnetics*, vol. 13, no. 5, pp. 401–411, 1992.

[12] P. Kędzia, T. Czechowski, M. Baranowski, J. Jurga, and E. Szcześniak, "Analysis of uniformity of magnetic field generated by the two-pair coil system," *Appl. Magn. Reson.*, vol. 44, no. 5, pp. 605–618, 2013.

[13] M. W. Garrett, "Table of solenoids with sixth-order error and near-maximum power efficiency," *J. Appl. Phys.*, vol. 40, no. 8, pp. 3171–3179, 1969.

[14] M. W. Garrett, "Polygonal coil systems for magnetic fields with homogeneity of the fourth to the eighth order," *Rev. Sci. Instrum.*, vol. 42, no. 6, pp. 840–857, 1971.

[15] D. M. Ginsberg and M. J. Melchner, "Optimum geometry of saddle shaped coils for generating a uniform magnetic field," *Rev. Sci. Instrum.*, vol. 41, no. 1, p. 122, 1970.

[16] H. Hanssum, "Exact solution of the Poisson equation for a DC current on a saddle-shaped Helmholtz coil," *Cell Res.*, vol. 16, no. 14, p. 3385, 1983.

[17] H. Hanssum, "The magnetic field of saddle-shaped coils. I. Symmetry of the magnetic field around the coil centre," *J. Phys. D, Appl. Phys.*, vol. 17, no. 1, p. 1, 1984.

[18] H. Hanssum, "The magnetic field of saddle-shaped coils. II. Transverse components," *J. Phys. D, Appl. Phys.*, vol. 18, no. 10, pp. 1971–1978, 1985.

[19] H. Hanssum, "The magnetic field of saddle-shaped coils. III. Improving the uniformity of mod B mod in a large volume," *J. Phys. D, Appl. Phys.*, vol. 19, no. 4, pp. 493–501, 1986.

[20] R. Turner, "A target field approach to optimal coil design," *J. Phys. D, Appl. Phys.*, vol. 19, no. 8, pp. L147–L151, 1986.

[21] W. Liu, D. Zu, X. Tang, and H. Guo, "Target-field method for MRI biplanar gradient coil design," *J. Phys. D, Appl. Phys.*, vol. 40, no. 15, pp. 4418–4424, 2007.

[22] J. Wang, B. Zhou, W. Wu, L. Chen, and J. Fang, "Uniform field coil design based on the target-field method in miniature atomic sensors," *IEEE Sensors J.*, vol. 19, no. 8, pp. 2895–2901, Aug. 2019.

[23] B. J. Fisher, N. Dillon, T. A. Carpenter, and L. D. Hall, "Design of a biplanar gradient coil using a genetic algorithm," *Magn. Reson. Imag.*, vol. 15, no. 3, pp. 369–376, 1997.

[24] Q. Wang, *Practical Design of Magnetostatic Structure Using Numerical Simulation*. Singapore: Wiley, 2013.

[25] Y. Li, Q. Wang, X. Zhu, Z. Ni, and L. Wang, "Decoupling design of Z2 superconducting shim coils for 9.4-T MRI superconducting magnet," *IEEE Trans. Appl. Supercond.*, vol. 26, no. 4, Jun. 2016, Art. no. 4403105.

[26] Z. Ni, L. Li, G. Hu, C. Wen, X. Hu, F. Liu, and Q. Wang, "Design of superconducting shim coils for a 400 MHz NMR using nonlinear optimization algorithm," *IEEE Trans. Appl. Supercond.*, vol. 22, no. 3, Jun. 2012, Art. no. 4900505.

[27] Q. Wang, G. Xu, Y. Dai, B. Zhao, L. Yan, and K. Kim, "Design of open high magnetic field MRI superconducting magnet with continuous current and genetic algorithm method," *IEEE Trans. Appl. Supercond.*, vol. 19, no. 3, pp. 2289–2292, Jun. 2009.

[28] C. C. Sanchez, M. F. Pantoja, and R. G. Martin, "Design of gradient coil for magnetic resonance imaging applying particle-swarm optimization," *IEEE Trans. Magn.*, vol. 47, no. 12, pp. 4761–4768, Dec. 2011.

[29] M. Poole and R. Bowtell, "Novel gradient coils designed using a boundary element method," *Concepts Magn. Reson. B, Magn. Reson. Eng.*, vol. 31B, no. 3, pp. 162–175, 2007.

[30] P. T. While, M. V. Meissner, and J. G. Korvink, "Insertable biplanar gradient coils for magnetic resonance microscopy: Theoretical minimization of power dissipation for different fabrication methods," *Biomed. Phys. Eng. Express*, vol. 4, no. 3, 2018, Art. no. 035019.
[31] J. Kennedy and R. Eberhart, "Particle swarm optimization," in *Proc. Int. Conf. Neural Netw. (ICNN)*, Nov./Dec. 1995, pp. 1942–1948.
[32] Y. Shi and R. Eberhart, "A modified particle swarm optimizer," in *Proc. IEEE World Congr. Comput. Intell.*, May 1998, pp. 69–73.

WENFENG WU received the master's degree in mechanical engineering from Shanghai University, China, in 2014. He is currently pursuing the Ph.D. degree with the School of Instrumentation and Optoelectronic Engineering, Beihang University. His research interests include the magnetic coil, magnetic shielding, and atomic magnetometers.

BINQUAN ZHOU was born in Shanxi, China, in 1981. He received the Ph.D. degree in precision instrument and mechanics from Beihang University, in 2017, where he is currently an Assistant Professor with the School of Instrumentation Science and Optical Engineering. He has undertaken multiple national and ministerial research projects, including the National Natural Science Fund, the 863 of Ministry of Science and Technology, and so on. His research interests include atomic gyroscope, atomic magnetometer, and MEG research.

ZHANCHAO LIU received the B.S. and Ph.D. degrees in precision instrument and machinery from the School of Instrumentation and Optoelectronic Engineering, Beihang University, Beijing, China, in 2007 and 2015, respectively, where he is currently an Assistant Professor. His current research interests include SERF magnetometer, atomic gyroscope, inertial navigation, and integrated navigation.

JING WANG was born in Baoding, Hebei, China, in 1993. She received the B.S. degree from the School of Mechanical Engineering, Hebei University of Technology, Tianjin, China, in 2015. She is currently pursuing the Ph.D. degree with the School of Instrumentation Science and Optoelectronics Engineering, Beihang University, Beijing, China. Her main research interests include uniform field coil design, inertial and magnetic measurements, atomic magnetometer, and MEG research.

HAOYING PANG received the B.S. degree in automation from the China University of Petroleum, China, in 2017. She is currently pursuing the Ph.D. degree with the School of Instrumentation and Optoelectronic Engineering, Beihang University. Her current research interests include magnetic field compensation and magnetic noise analysis of atomic spin sensors.

LINLIN CHEN received the Ph.D. degree from Beihang University, in 2018. She is currently a Lecturer with the Department of Aerospace Science and Technology, Space Engineering University. Her research interests include atomic gyroscope, atomic magnetometer, and electronic-optical detection technology.

WEI QUAN received the Ph.D. degree from Beihang University, in 2008, where he is currently a Professor with the School of Instrumentation and Optoelectronic Engineering. His research interests include celestial navigation and the recently developed atomic inertial sensors based on alkali-metal vapor cell.

GANG LIU received the B.S. and M.S. degrees from Shandong University, China, in 1992 and 1998, respectively, and the Ph.D. degree from the Dalian University of Technology, China, in 2001. He is currently a Ph.D. Supervisor with the School of Instrumentation and Optoelectronic Engineering of Beihang University. His research interests include magnetic suspension technology, spacecraft attitude control, and high sensitivity atomic magnetometers.